Nuclear Inst. and Methods in Physics Research, A 1049 (2023) 168126

Contents lists available at ScienceDirect

Nuclear Inst. and Methods in Physics Research, A

journal homepage: www.elsevier.com/locate/nima

Full Length Article

TOFu: A fully digital data acquisition system upgrade for the neutron time-of-flight spectrometer TOFOR

B. Eriksson [a,*], S. Conroy [a], G. Ericsson [a], J. Eriksson [a], A. Hjalmarsson [a], M. Weiszflog [a], Z. Ghani [b], M. Maslov [b], JET Contributors [1]

[a] Department of Physics and Astronomy, Uppsala University, Lägerhyddsvägen 1, Uppsala, 752 37, Sweden
[b] UKAEA, Culham Centre for Fusion Energy, Culham Science Centre, Abingdon, OX14 3DB, United Kingdom

ARTICLE INFO

Keywords:
TOFOR
Data acquisition system
TOFu
Time-of-flight
Neutron spectrometry
Joint European Torus

ABSTRACT

TOFOR is a time-of-flight (TOF) neutron spectrometer located at the Joint European Torus (JET) with a vertical sightline of the JET plasma. It consists of 5 *start* (denoted S1) and 32 *stop* (denoted S2) plastic scintillation detectors which can be used in coincidence to generate a TOF spectrum. Spectroscopic analysis of the neutron TOF spectra produced by the JET plasma is regularly performed to determine, e.g., the fuel ion ratio and the presence of fast ion species in the fusion plasma. TOFOR has been upgraded with a new digital data acquisition (DAQ) system, denoted TOFu, which consists of 10 waveform digitizers with a total of 40 channels, 37 of which are connected to the photomultiplier output of the different S1 and S2 detectors. This paper presents a technical overview of the TOFu system and describes the offline analysis capabilities of TOFu which were not available with the previous DAQ system. Two experimental JET discharges are studied and used to show that the signal-to-background ratio is improved by almost 200% for the 2.5 MeV neutron signal and almost 400% for the 14 MeV neutron signal using the new offline analysis capabilities.

1. Introduction

TOFOR [1,2] is a time-of-flight (TOF) neutron spectrometer with a collimated vertical view of the Joint European Torus (JET) fusion plasma. It is comprised of two sets of plastic scintillation detectors as shown in the left panel of Fig. 1. The first set consists of five thin cylindrical scintillators, denoted S1-01 to S1-05, which are placed on the axis of the collimator and provide the start signals for the TOF measurement. The second set of 32 scintillators, denoted S2-01 to S2-32, are placed at a distance of approximately 1.2 m upstream of the S1 stack symmetrically around the collimator axis in the φ direction indicated in the figure and provide the stop signals for the TOF measurement. The minimal and maximal scattering angles, $\alpha_{\min} = 23.0°$ and $\alpha_{\max} = 37.9°$, are shown in the figure together with the corresponding S1-S2 path lengths, $L(\alpha_{\min}) = 1304$ mm and $L(\alpha_{\max}) = 1157$ mm. The typical sequence resulting in a detected event in one of the sub-detectors can be described as (i) a fusion-born neutron scatters elastically on a proton in the scintillation material of the detector, transferring a fraction of its kinetic energy to the proton, (ii) the recoil proton interacts with the electronic structure of the detector material, part of the energy deposited to the proton is emitted as scintillation light, the intensity of which is related to the deposited energy, (iii) the scintillation light is guided to a photomultiplier tube (PMT) where the photons are converted to photoelectrons through the photoelectric effect, (iv) the photoelectrons are multiplied in the PMT through a chain of dynodes to an electric pulse which is fed directly into one of the channels of the data acquisition (DAQ) system. Consequently, the pulse amplitude, or more practically, the integral of the pulse waveform (here called the integrated charge of the pulse), can be correlated to the energy transferred from the neutron to the recoil proton in the detector. If a single neutron interacts both in an S1 and S2 detector, the neutron time-of-flight can be calculated from the pulse times-of-arrival. As is shown in Fig. 1, the S2 detectors are tilted with respect to the tangent of the sphere indicated in the figure by $\theta = 5°$ to partially compensate for the light transport time from the point of interaction to the PMT. The right panel of the figure shows the dimensions of the S1 and S2 sub-detectors.

Fusion-born neutrons from three different reactions involving deuterium (D) and tritium (T) constitute the main contribution to the neutron time-of-flight spectrum through (i) the DD reaction yielding 2.5 MeV neutrons, (ii) the DT reaction yielding 14 MeV neutrons, and (iii) the TT reaction yielding a continuum of neutron energies spanning 0–9.4 MeV. Examples of how neutrons from these reactions produce characteristic features in the TOF spectrum of TOFOR are

* Corresponding author.
E-mail address: benjamin.eriksson@physics.uu.se (B. Eriksson).
[1] See the author list of 'Overview of JET results for optimising ITER operation' by J. Mailloux et al. 2022 Nucl. Fusion 62 042026.

https://doi.org/10.1016/j.nima.2023.168126
Received 16 November 2022; Received in revised form 1 February 2023; Accepted 8 February 2023
Available online 10 February 2023

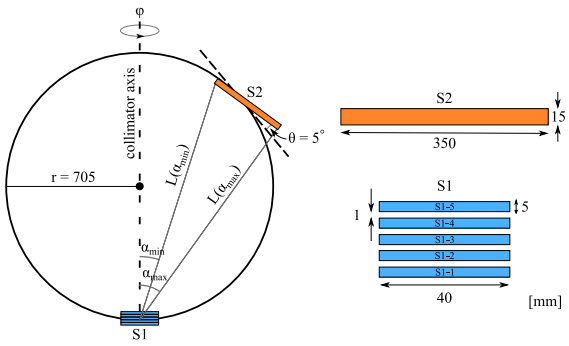

Fig. 1. Schematic view of TOFOR including the S1 stack and one of the 32 S2 detectors (left panel), including sub-detector dimensions (right panel). The figure is not to scale.

shown in Fig. 2 for three different JET Pulse numbers (JPN) with (a) a D-dominated plasma (JPN 95499), (b) a D-dominated plasma with trace amounts of T (JPN 98044), and (c) a T-dominated plasma with trace amounts of D (JPN 99134). Given the known geometry of TOFOR, DD neutrons are expected around $t_{TOF} = 65$ ns, DT neutrons around $t_{TOF} = 27$ ns, and TT neutrons at $t_{TOF} > 30$ ns. Further, a peak due to γ-rays is visible around $t_{TOF} = 4$ ns given by the constant speed of light. TOFOR has been used to determine various fusion-relevant plasma parameters in many physics studies, such as [3–8], since its installation in 2005 [1]. An upgrade of the TOFOR DAQ system denoted TOFu has been conducted to improve the spectroscopic capability of TOFOR. This involves the procurement and installation of fully digital waveform digitizers, allowing for correlated time and pulse height analysis of the acquired data which was not possible with the original DAQ system.

This paper presents a technical overview of TOFu including information on the DAQ hardware, analysis software, and the control and monitoring system (presented in Section 2), as well as some details of the post-processing of the data, including the employed pulse time pick-off method (Section 3) and the algorithm for finding coincidences in the data (Section 4). The energy calibration of the TOFu system is presented in Section 5 and is used in Section 6 to improve the signal-to-background ratio of TOFOR using kinematic cuts. Improvements to the TOFOR response function are presented in Sections 7 and 8, where the energy-dependent time resolution and acquisition energy thresholds are determined. Finally, a comparison between the new and original DAQ system is presented in Section 9, along with some concluding remarks in Section 10.

2. Technical details

The TOFu DAQ system was implemented in two phases. In the first phase a prototype system was tested using five ADQ412 digitizer boards procured from Teledyne SP Devices[2] [10]. In the second phase, the full system was implemented with an additional five boards from the same company. By this time Teledyne SP Devices had developed the ADQ14 digitizer which was deemed more suitable for the TOFu application. The TOFu DAQ system, thus, consists of ten digitizer boards procured from Teledyne SP Devices: five ADQ412 boards with 12 bits vertical resolution and five ADQ14AC boards with 14 bits vertical resolution housed in an 18-slot Adlink[3] PXIe-2780 chassis. Each board has four input channels amounting to a total of 40 channels, accommodating the 37 TOFOR sub-detector output channels. The entire DAQ system occupies a space of 46 cm (width) × 19 cm (height) × 47 cm (depth) fitting in a single 3U height rack in the DAQ cubicle. The digitizers are set up and run using the API provided by Teledyne SP Devices. The ADQ14AC digitizers are equipped with the FWPD pulse detection

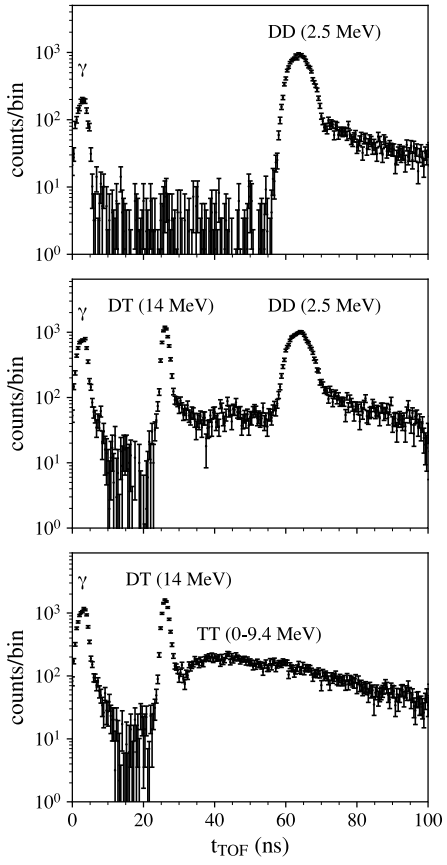

Fig. 2. Examples of time-of-flight spectra measured by TOFOR for (a) a D-dominated plasma (JPN 95499), (b) a D-dominated plasma with trace amounts of T (JPN 98044), and (c) a T-dominated plasma with trace amounts of D (JPN 99134). Peaks corresponding to neutrons produced in DD, DT, and TT reactions are indicated in the figure as well as the γ-ray peak.
Source: Figure from [9].

firmware package [11] and are run using a modified version of the disk streaming application written in C available with the FWPD option, whereas the ADQ412 digitizers are run using a Python application. The API allows us to control a large number of parameters such as record lengths, bias levels, trigger levels, and the data acquisition duration to mention a few. TOFu acquires data from the 37 detector channels independently of each other using a fixed (pre-set) individual trigger level for each channel. All digitizer boards have a shared timing, synchronized through phase lock loops to the chassis back-plate. Further, JET utilizes a central Control and Data Acquisition System (CODAS) to initialize and synchronize the various diagnostic instruments to a common JET time. An overview of the sequence of an experimental JET discharge for TOFu is shown in Fig. 3. When an experimental discharge is started, CODAS sends a signal containing the JET pulse number (pulse.ini) and initialization parameters (KM11D.ini) which are read by the TOFu DAQ system and used to set, e.g., record lengths and bias levels. Once the boards have been initialized they are armed and wait for the signal from CODAS to either abort the shot (abort.abt) if the initialization of the JET machine was unsuccessful or to start acquiring data (PRE). The PRE signal is sent to all JET diagnostics and ensures that the different instruments are synchronized to a common JET time to allow for time-resolved comparisons between the systems. The data saved by TOFu consists of board temperature readings, time stamps (including the offset time at which PRE was detected), and pulse waveforms. Finally, the data acquired by TOFu is transferred to a server managed by CODAS. For the TOFu system, the boards digitize incoming pulse waveforms at a frequency of 1 GHz, saving 64 samples (i.e. a total

[2] www.spdevices.com
[3] www.adlinktech.com

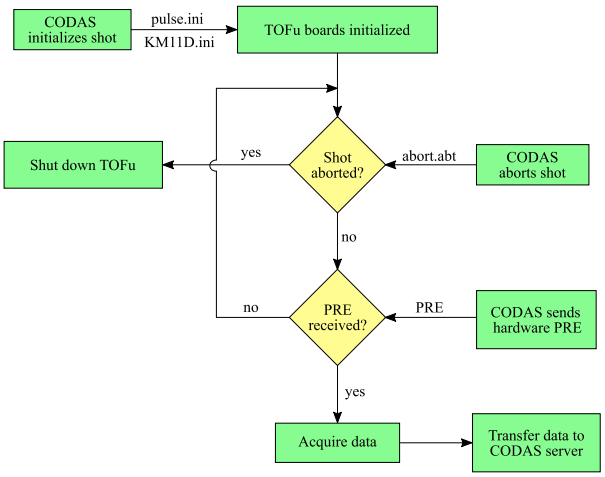

Fig. 3. Flowchart of the discharge sequence for the TOFu system.

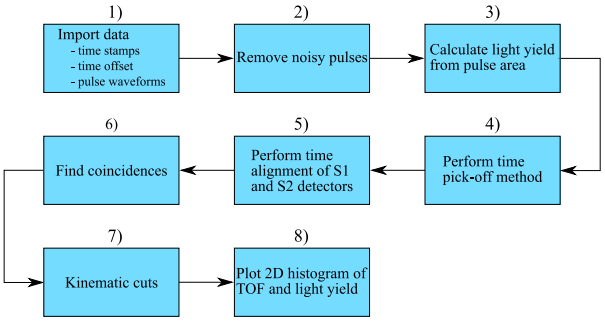

Fig. 4. Flowchart of the main processes performed by the TOFu analysis software.

of 64 ns) per record with the ADQ14 boards and 56 samples per record with the ADQ412 boards, 16 of which are pre-trigger samples, as well as the trigger time stamp. This allows for detailed pulse shape analysis during the post-processing of experimental data.

2.1. TOFu analysis software

The software for the post-processing of the data to create time-of-flight spectra was developed in Python and is publicly available at [12]. The main steps in the analysis chain are shown in Fig. 4 and involve (1) importing the data for a given JET pulse number from the JET servers. This includes the trigger time stamps, the digitized pulse waveform, and the offset time used for the time alignment procedure of the different sub-detectors. (2) Oddly shaped pulse waveforms are removed, this includes waveforms with baselines fluctuating outside a nominal value and waveforms with negative areas. (3) The light yield associated with the pulse area is calculated for all records. The light yield calibration is further discussed in Section 5. (4) The pulse time of arrival is determined using the method discussed in Section 3. (5) Due to differences in cable lengths and signal processing pathways all S1 and S2 sub-detectors must be time-aligned according to the method presented in [13]. (6) Coincidences between the S1 and S2 detectors are found using the method described in Section 4. (7) Kinematic cuts are applied to the TOF and light yield data, this is further discussed in Section 6. (8) The 2D time-of-flight and light yield histogram is plotted.

2.2. Control and monitoring system

The TOFOR spectrometer is equipped with a control and monitoring system (C&M) which consists of two pulsed light emitting sources: a 438 nm blue light LED and a 531 nm green light neodymium-doped lanthanum scandium borate (Nd:LSB) laser. The light sources are connected to each TOFOR photomultiplier tube by optical fiber cables. The LED emits light at a fixed intensity and is used mainly for monitoring PMT gain drifts whereas the laser is equipped with a motorized polarizer enabling the possibility of varying the emitted light intensity. The laser system is set up to mimic the pulse waveforms created by the scintillation light from the plastic scintillators of the TOFOR sub-detectors. Consequently, it is possible to perform pulse amplitude-dependent analyses of various aspects of the TOFu system in a controlled manner using the laser system. The laser C&M system is, e.g., utilized to measure the energy-dependent timing resolution described in Section 7. The LED and laser C&M systems are described in detail in [14,15].

3. Time pick-off method

The ADQ cards have a sampling frequency of 1 GHz and employ a constant trigger level (shown by the dash-dotted line in Fig. 5). The recorded time stamp (i.e., the time since PRE was detected by the ADQ card) of a pulse digitized by the system is thus associated with a single sample exceeding the trigger level and is recorded with a precision of 1 ns. A time pick-off method is used to determine the pulse time of arrival at a sub-nanosecond level and to reduce the pulse timing uncertainty due to the amplitude walk associated with employing a constant trigger level to pulses of different amplitudes. The utilized method is shown in Fig. 5 and described below. The electric pulse caused by the scintillation light is sampled at a frequency of 1 GHz giving one sample (represented by the blue dots) per nanosecond. A Whittaker–Shannon (W–S) interpolation [16], shown as the blue dashed line in the figure, is applied to the $m = 64$ (or $m = 56$) sampled points,

$$Y(t_{\mathrm{u}}) = \sum_{i=1}^{m} \mathrm{sinc}\left(\frac{t_{\mathrm{u}} - t_i}{\Delta t}\right) y_i\,, \tag{1}$$

reproducing the original signal $Y(t_{\mathrm{u}})$ where t_{u} is a linearly spaced time-vector that has been up-sampled by a factor 10, t_i is the time of a sampled point at an amplitude of y_i ADC codes, and $\Delta t = 1$ ns is the sampling period. Up-sampling the pulse allows us to with greater precision determine the total accumulated charge of the pulse which is associated with the deposited energy in the scintillation detector. It also allows us to perform the offline time pick-off method to obtain the time of arrival of the waveform. The time of arrival is determined by finding a constant fraction (north-facing triangle in Fig. 5) of the up-sampled pulse peak amplitude (black cross). In the figure, the constant fraction is set to 1/3 for illustrative reasons, in reality, it may be chosen freely and is typically set to 5%–10% for TOFu. A linear regression (red line) is performed around the points closest to the constant fraction, and the time of arrival (south-facing triangle) is determined as the point at which the linear regression intersects the baseline (black dotted line). The new global time, t_{G}, of the pulse is given by adjusting the recorded time stamp with the determined time of arrival.

4. Method for finding coincidences

This section is to a large degree taken from [9] and is repeated here for the sake of completeness. Each record gathered by TOFu is attributed a global time stamp, t_{G}, using the time pick-off method discussed in Section 3. After the S1 and S2 sub-detectors have been aligned to each other, according to the method presented in [13], a search algorithm is applied to the data to find coincidences between S1 and S2 detectors. A coincidence, in the context of TOFu, is defined as any two events occurring within a user-defined time window, Δt_{TOF}, in two different detectors, or in the same detector. Further, coincidences can be categorized either as true coincidences, in which a single particle is responsible for the two events, or random coincidences, in which two

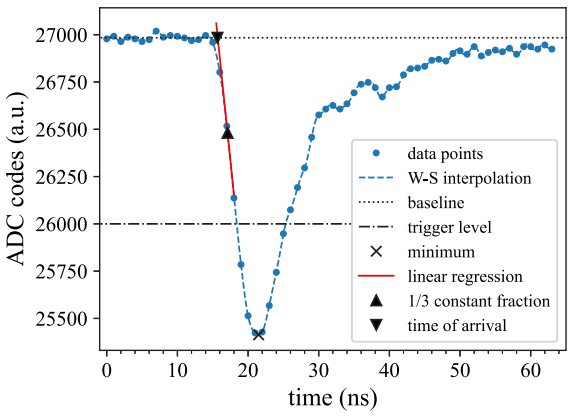

Fig. 5. Typical ADQ14 digitized scintillation pulse sampled at 1 GHz (blue dots) with a Whittaker–Shannon (W–S) interpolation indicated by the blue dashed line. The baseline at 27k ADC codes is indicated by the dotted black line and the trigger level at 26k ADC codes is shown as a dash-dotted line. The minimum of the W–S interpolation is shown as a black cross, and a corresponding constant fraction of 1/3 of the minimum is indicated by the north-facing triangle. A linear regression around the constant fraction, given by the red line, gives the pulse time of arrival indicated by the south-facing triangle.
Source: Figure from [9].

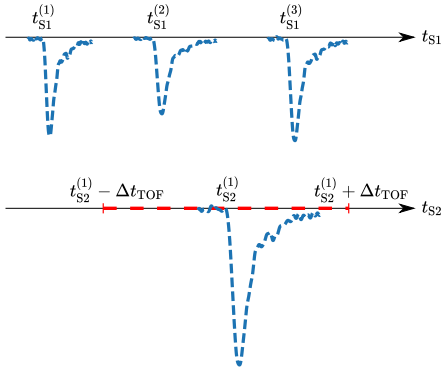

Fig. 6. Two detector timelines with a number of detected events. The coincidence time window is shown on top of the S2 timeline (red dashed line) for a user-defined time window Δt_{TOF}.
Source: Figure from [9].

different particles happen to interact in the detector(s) within the given time window. There is no way of knowing which category a coincidence falls under, however, by finding coincidences between S1 and S2 sub-detector combinations, a time-of-flight spectrum can be calculated in which the peaks corresponding to true coincidences can be discerned. An example of how the flight time is calculated is shown in Fig. 6. Two timelines corresponding to an S1 and S2 detector are displayed. Three events in the S1 detector are shown at times $t_{\mathrm{S1}}^{(1)}$, $t_{\mathrm{S1}}^{(2)}$ and $t_{\mathrm{S1}}^{(3)}$ along with one event on the S2 timeline $t_{\mathrm{S2}}^{(1)}$. In the search algorithm, the S2 event is selected, and the user-defined time window is calculated by $t_{\mathrm{S2}}^{(1)} \pm \Delta t_{\mathrm{TOF}}$, shown in the figure as the red dashed line. Two of the events on the S1 timeline can be found within the time window yielding two coincidences with the interaction time differences (times-of-flight) $t_{\mathrm{S2}}^{(1)} - t_{\mathrm{S1}}^{(2)}$ and $t_{\mathrm{S2}}^{(1)} - t_{\mathrm{S1}}^{(3)}$. Repeating the analysis on all events for the given S1-S2 detector combination and plotting the data as a histogram results in a TOF spectrum.

5. Light yield calibration

The TOFu system acquires digitized waveform information, such as the waveform shown in Fig. 5. The integral of each waveform is correlated with the amount of scintillation light incident on the PMTs connected to each TOFOR scintillation sub-detector. Further, the amount of produced scintillation light is related to the energy deposited by the particle interacting in the detector through a non-linear light yield function (Eq. (5)). For a neutron spectrometer such as TOFOR, the main process of interest is the elastic scattering of a neutron on a proton in the scintillation material. The amount of kinetic energy transferred from the neutron to the proton in the scattering process gives an upper limit to the amount of scintillation light the recoil proton may produce in the detector material. In such a way, the light yield spectrum from recoil protons yields information regarding the neutron energy distribution incident on the detector. A light yield calibration using a Na-22 source is performed to translate the integral of a digitized waveform to light yield. The light yield calibration is required to apply kinematic cuts (discussed in Section 6) to the experimental data, as well as for applying the appropriate detection energy thresholds (discussed in Section 8) to the detector response function.

Na-22 decays through the emission of a positron to Ne-22, predominantly through an excited state of Ne-22 which promptly de-excites through the emission of a 1275 keV photon to the ground state. Additionally, 511 keV photons are produced through the annihilation of the positron with an electron. The photons give rise to distinct Compton spectra when observed with detectors sensitive to γ-particles, such as plastic scintillators. The (integrated) pulse height spectrum acquired with the S2-01 sub-detector when exposed to the radiation of a Na-22 source is shown in panel (a) of Fig. 7. The integral of an acquired waveform is calculated numerically using trapezoidal integration. Two Compton edges (indicated by the arrows) corresponding to the two gamma energies are visible in the figure. The same setup is simulated in MCNP 6.2 [17,18] with the raw results shown in panel (b) of Fig. 7. As no resolution broadening is applied to the simulated spectrum in the figure, sharp Compton edges (around 350 and 1100 keV) and the 1275 keV photopeak are visible. The 511 keV photopeak is obscured by the 1275 keV Compton continuum.

5.1. Fitting procedure

In order to translate the integral of a waveform to the corresponding light yield, the light yield function for γ-particles is assumed to follow a one-to-one correspondence. A fitting procedure is then performed on the experimental and simulated spectra for each TOFOR sub-detector. The aim of the exercise is to yield an offset ω and a multiplier μ for the given sub-detector which may be used in the form

$$E_{\mathrm{ee}}(Q) = \omega + \mu Q\,, \tag{2}$$

where E_{ee} is the light yield given in units of electron equivalent (ee) energy and Q is the integral of the pulse waveform. This is achieved by applying two parameters to adjust the intensity of the 511 keV and 1275 keV component of the simulated spectrum, I_{511} and I_{1275}, and a Gaussian broadening with a width

$$\sigma = \frac{d\Lambda}{2\sqrt{2\ln 2}}\,, \tag{3}$$

where the resolution function $d\Lambda/\Lambda$ is determined using the parameterization [19]

$$\frac{d\Lambda}{\Lambda} = \sqrt{\alpha^2 + \frac{\beta^2}{\Lambda} + \frac{\gamma^2}{\Lambda^2}}\,, \tag{4}$$

where Λ is the simulated light yield in the detector. Finally, the offset ω and multiplier μ are applied to the horizontal axis of the experimental spectrum. This results in a total of seven fit parameters which are varied to adjust the MCNP spectrum (I_{511}, I_{1275}, α, β, and γ) and the horizontal experimental axis (ω and μ) to minimize the χ^2 for the simulated and experimental spectra. The code used for the calibration is available in [20]. Four (out of 37) of the resulting spectra after performing the minimization are shown in Fig. 8, where the experimental gamma spectra with new horizontal axes are shown as black points with the

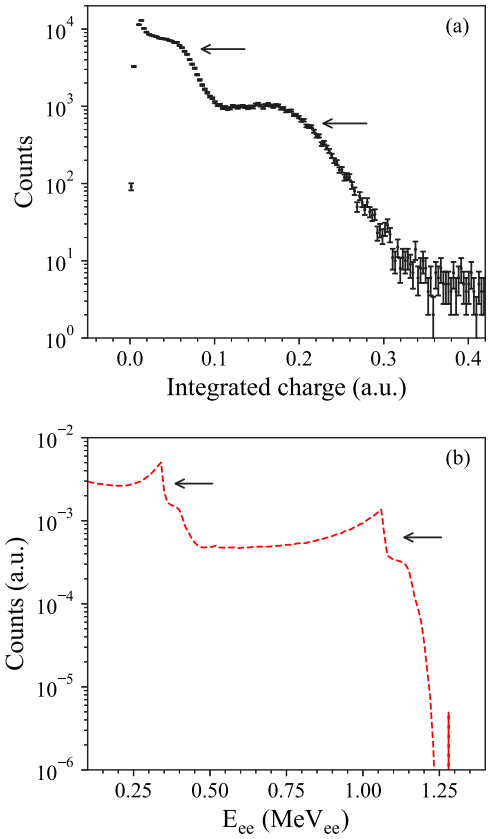

Fig. 7. (a) Na-22 gamma spectrum acquired with the S2-01 sub-detector. Two Compton edges are indicated by the arrows. (b) The same detector is simulated in MCNP 6.2. No broadening has been applied to the simulated spectrum.

Table 1
Coefficient values for Eq. (5). E_p is in units of MeV.

	κ_1	κ_2	κ_3	κ_4
$0 < E_p \leq 1.9$	0	0.0469	0.1378	−0.0183
$1.9 < E_p \leq 9.3$	−0.0142	0.1292	0.0697	−0.00315
$9.3 < E_p \leq 18.9$	−1.8899	0.7067	0	0

corresponding light yield calibration fit shown as the blue dash-dotted lines. The orange line represents the background spectrum which is acquired without the source in place for the same amount of time as for the ^{22}Na measurements (five minutes for each S2 and nine hours for the S1 stack). It is used as a fixed component in the fitting procedure. Since the installation of TOFu, energy calibrations have been performed approximately once per year. The system exhibits good stability between calibrations. By determining an offset ω and multiplier μ for each sub-detector and using Eq. (2) for translating integrated pulse charge to light yield, it is possible to calculate the proton recoil energy spectrum given a proton light yield function. The proton recoil energy is calculated in the TOFu system by inverting a light yield function with the form

$$E_{ee} = \kappa_1 + \kappa_2 E_p + \kappa_3 E_p^2 + \kappa_4 E_p^3 , \tag{5}$$

where the light yield (E_{ee}) and proton recoil energy (E_p) are given in units of MeV_{ee} and MeV respectively. The coefficients take the values provided in Table 1 for the different ranges of proton recoil energy. Now that we have a method for converting the integrated charge of a pulse waveform to the corresponding proton recoil energy, we can make use of kinematic cuts as a background discrimination technique and apply appropriate energy thresholds to the detector response function.

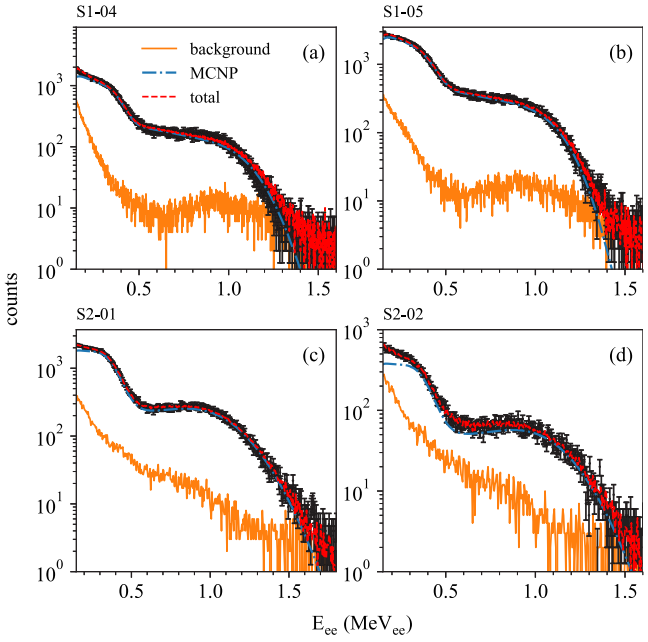

Fig. 8. Na-22 gamma spectra acquired for detectors (a) S1-04, (b) S1-05 (c) S2-01, (d) S2-02 shown as black points with the corresponding background spectrum shown as the orange line and the light yield calibration fit shown as the blue dash-dotted line. The sum of the fit and the background spectrum is given as the red dashed line.

6. Kinematic cuts

Given the known geometry of TOFOR, it is possible to calculate the maximal and minimal angles ($\alpha_{max} = 37.9°$ and $\alpha_{min} = 23.0°$) in the S1 stack which result in neutrons scattering in the direction of an S2, as indicated in Fig. 1. Associated with these angles there is a path length, $L(\alpha_{min}) = 1304$ mm and $L(\alpha_{max}) = 1157$ mm, corresponding to the two edges of an S2 detector. For a given flight time, t_{TOF}, one can calculate an upper and lower limit of the possible energy transfer from a neutron incident on the S1 stack to a proton in the scintillator material, as is exemplified in [21]. These are given by

$$E_{min}^{S1} = \frac{m_n}{2}\left(\frac{L(\alpha_{min})}{t_{TOF}}\right)^2 \tan^2\alpha_{min} , \tag{6}$$

and

$$E_{max}^{S1} = \frac{m_n}{2}\left(\frac{L(\alpha_{max})}{t_{TOF}}\right)^2 \tan^2\alpha_{max} . \tag{7}$$

For the interaction in an S2 detector, there is no restriction in the scattering angle, the neutron may deposit anything from all to none of its energy in the detector material. Consequently, it is not possible to set a lower limit on the energy transferred to the S2 detector material. It is however possible to infer an upper limit by considering the neutrons which deposit the least possible amount of energy in an S1 while scattering toward an S2. The upper limit is then

$$E_{max}^{S2} = \frac{m_n}{2}\left(\frac{L(\alpha_{min})}{t_{TOF}}\right)^2 . \tag{8}$$

The kinematic limits can be passed through the light yield function (Eq. (5)) and applied to the measured light yield vs. TOF spectrum as exemplified in Fig. 9. The upper and lower S1 limits are shown as red lines in panel (a), correspondingly, the upper S2 limit is shown in panel (b). The projection onto the time-of-flight axis when the cuts are applied is shown in panel (c) and includes the events located

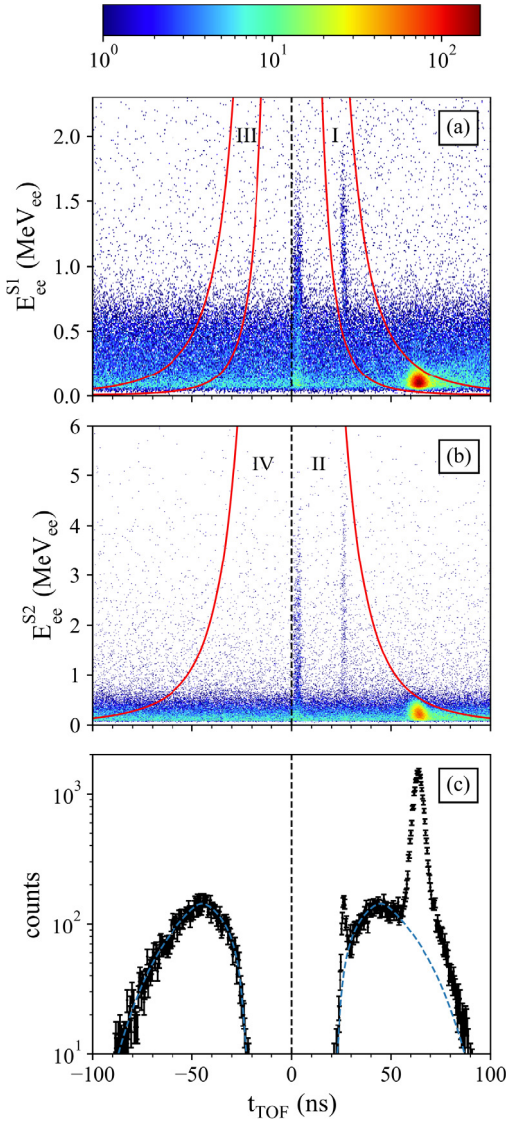

Fig. 9. Experimental neutron spectra of JPN 100850 acquired by the TOFu system. The top two panels show the two-dimensional histograms for the measured times-of-flight (on the horizontal axis) and light yields (on the vertical axis) where the vertical axes correspond to the (a) S1 detectors and (b) S2 detectors. The kinematic cuts are included as red lines. The projection onto the TOF axis when the cuts are applied is shown in panel (c) including the estimated background component (blue dashed line).

within both the areas indicated by the numerals I and II in the figure. Random coincidences are expected across the entire TOF spectrum. These constitute an unavoidable background component and can be seen in panels (a) and (b) by extending the TOF axis to negative flight times where nothing but random coincidences is expected. An estimate of the random coincidence component can be made by mirroring the kinematic cuts to negative flight times. Events located within the areas indicated by the numerals III and IV are projected onto the TOF axis and are shown as the black points at negative times-of-flight. An estimate of the random coincidence component, shown as the blue dashed line, can subsequently be made. The estimate is performed by averaging the negative side of the 2D histograms along the TOF axis for both the S1 and S2 detectors yielding a smoothed background spectrum. By applying the mirrored kinematic cuts to the smoothed background spectrum and projecting the result onto the TOF axis, the blue dashed line is obtained. The procedure is further described in [21].

7. Time resolution

The timing resolution at which coincidence measurements between two sub-detectors can be made is an important parameter to determine for a time-of-flight system such as TOFOR to properly model the detector response function. Several aspects must be taken into account to appropriately broaden the response function. Some broadening effects are taken into account by the particle transport code used to generate the response function. Such effects include the geometry of the system, multiple scattering of neutrons in the detectors, light transport of scintillation light to the PMTs, and the detection efficiency due to reaction cross sections. Other effects must be applied to the response function *a posteriori*, e.g., detection energy thresholds (described in Section 8), and the intrinsic timing resolution of the chain of electronics starting with the time jitter in the PMTs, followed by the fan-in-fan-out (FIFO) modules and the signal processing pathways in the ADC cards. A final time broadening effect arises from the precision of the time pick-off method in determining the pulse time of arrival. Instead of disentangling the contribution of these different effects to the time broadening, we measure the combined broadening accumulated by the intrinsic timing resolution and the precision of the time pick-off method. Further, we can expect a pulse amplitude dependency on the timing resolution. Thus, the goal is to measure the timing resolution of each sub-detector as a function of pulse height, or equivalently, light yield (by using the method outlined in Section 5).

The timing resolution is measured by utilizing the laser C&M system (described in 2.2). Laser pulses of varying intensities are fired at each S1 and S2 PMT. Given the similarity of the pulse waveforms between the laser pulses and actual scintillation light from experiments, the laser pulse integral can be translated to a corresponding light yield using Eq. (2). For each fired laser pulse, a synchronization signal from the laser C&M system is cloned and fed directly into two unoccupied DAQ channels. Light yield-dependent coincidence measurements can then be performed between any given sub-detector and one of the synchronization channels. An example of such coincidence measurements for sub-detector S2-01 is shown in panel (a) of Fig. 10 for three different laser intensities corresponding to 275, 475, and 675 keV$_{ee}$. As expected, the time difference between the laser pulses and their corresponding synchronization signals is distributed around $\Delta t_L = 0$ as they are fired from the C&M system simultaneously. The widths of the distributions yield information on the timing resolution of the system. However, to calculate the timing resolution for the specific sub-detector, the contribution from the synchronization signal of widening the distributions must be estimated. For this purpose, the second synchronization signal is used to record the time difference between all pairs of cloned signals. The standard deviation of the yielded distribution is calculated to $\sigma_{synch} = 36$ ps and is indicated in the figure. Finally, σ_{synch} is subtracted from the widths found in panel (a). In panel (b) the result of this exercise is shown for all the utilized laser intensities (light yields) for the same sub-detector as in (a). By fitting a function on the same form as Eq. (4) we obtain an estimate of the timing resolution of the sub-detector as a function of light yield. The method is then repeated for all S1 and S2 sub-detectors. The time resolution analysis code is available in [22].

8. Energy thresholds

Determining the energy thresholds of the TOFu system is necessary to correctly apply energy cut-off limits to the detector response function. The energy detection threshold for each S1/S2 sub-detector is limited by the amount of scintillation light produced in the detector material for a given recoil proton energy, as well as the ability to effectively transport the light to the PMTs. Further, the user-defined DAQ hardware trigger levels (exemplified in Fig. 5 as a black dash-dotted line at 26k codes) set a lower pulse height limit, or correspondingly, a lower energy limit, at which events can be recorded. The fully digital

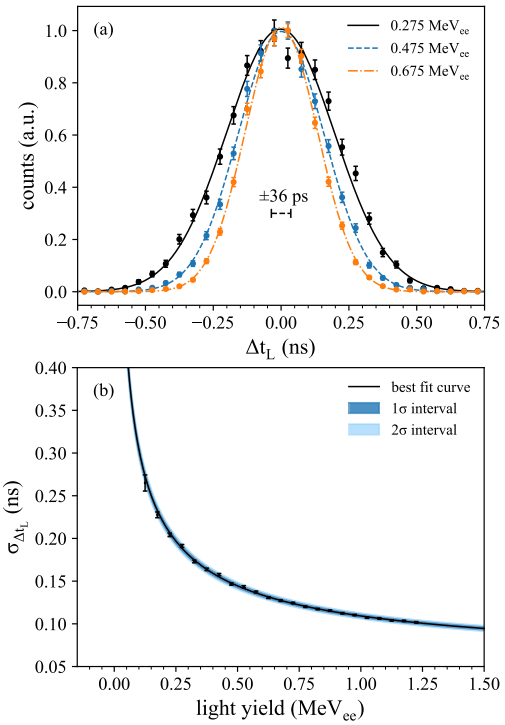

Fig. 10. (a) Histogram of time differences between laser pulses and synchronization signal (points) with Gaussian fits (lines) for three different light yields for sub-detector S2-01. The standard deviation (36 ps) of the distribution given by looking at time differences between the two synchronization channels is indicated in the figure. (b) Time resolution as a function of light yield (black points) including fit (black line) with confidence levels (blue shaded regions).

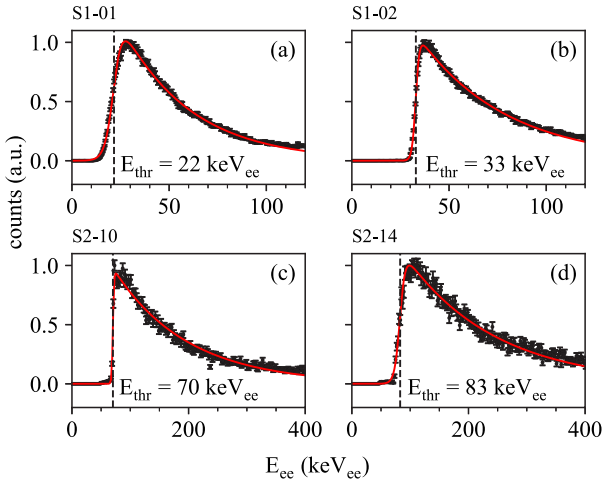

Fig. 11. Light yield spectra of two S1 detectors (top panels) and two S2 detectors (bottom panels). The product of the logistic function and an exponential are fit to the data (red line). Thresholds (black dashed lines) are defined as the mid-point of the logistic function and are determined to (a) 22 keV_{ee}, (b) 33 keV_{ee}, (c) 70 keV_{ee}, and (d) 83 keV_{ee}.

nature of the TOFu DAQ system makes it possible to apply arbitrary thresholds in the post-analysis of the data, with the limitation that they must be higher or equal to the detection thresholds determined by the trigger setting of the DAQ. Given that we want to make use of as much of the acquired data as possible, we determine the energy thresholds corresponding to the DAQ hardware trigger settings and use these in the post-analysis of the experimental data as well as in the detector response function.

The procedure for determining the hardware energy thresholds for the 37 detectors of TOFOR is illustrated in Fig. 11. Thresholds for the S1 detectors are determined by making use of the Na-22 gamma spectra and light yield calibrations presented in Section 5. The low-energy regions of the Na-22 spectra for two S1 sub-detectors are shown in panels (a) and (b) in Fig. 11. A fit, $f = f_1 \cdot f_2$, is applied to the spectrum where f_1 is the logistic function,

$$f_1\left(E_{ee}\right) = \frac{\lambda}{1 + e^{-k(E_{ee} - E_{thr})}}, \tag{9}$$

representing the electronic threshold action, and f_2 is an exponential,

$$f_2\left(E_{ee}\right) = ae^{-bE_{ee}}, \tag{10}$$

modeling the pulse height distribution. The free parameters for the fitting procedure are thus λ, k, E_{thr}, a, and b. In Eq. (9), λ determines the maximum value of the sigmoid, k corresponds to the steepness of the curve, and the energy threshold, E_{thr}, is defined as the sigmoid midpoint, shown as the black dashed line in the figure. The energy thresholds of the S2 detectors are determined similarly. However, due to a higher sensitivity to low energy background, we make use of experimental neutron data with kinematic cuts and an S1 coincidence requirement applied to produce the light yield spectra exemplified for two S2 sub-detectors in panels (c) and (d) of the figure. The energy threshold limits, E_{thr} are determined in the same way as for the S1 sub-detectors and are shown in the figure.

9. Improvements and comparison

One of the major advantages of a fully digital system such as TOFu is improved data availability. Since each acquired pulse waveform is saved we can easily investigate exactly what is being measured by the TOFOR system and can apply advanced pulse sorting algorithms, granting us more control over the data sets we process, increasing our confidence in the results from the physics analyses performed on the data. The purpose of the TOFu upgrade was not to improve the overall resolution of the system which is largely determined by the geometry of TOFOR, indeed, extracting the energy resolution from the improved detector response function for 2.5 MeV neutrons yields $dE_n/E_n = 7.9\%$ (full width at half maximum) which is in line with the previous response function [23].

TOFu has been run in parallel with the previous DAQ system for consistency checks. As shown in Fig. 12, the count rates for the new and old systems are similar to a large degree. The difference in efficiencies between the new and previous DAQ can be explained by different trigger settings and acquisition dead times. Count rates are, in addition, consistent with the count rates provided by the JET fission chambers [24]. Further, a prototype of the TOFu system has been extensively compared to the previous DAQ in, e.g., [10,25]. The fully upgraded TOFu system has also been utilized in studies (e.g., [8,13]) without making use of kinematic cuts and has been shown to provide results consistent with models and other diagnostic systems. Here we present some further improvements of the TOFu system compared to the original DAQ.

9.1. Dead time

The upgraded data acquisition system has an improved dead time compared to the original DAQ. The distribution of time differences, Δt_{S1}, between each acquired pulse waveform for the S1 sub-detectors is shown in Fig. 13 for TOFu and the original DAQ. The dead time of the two DAQ systems can be extracted from the sharp shoulder located at ~60 ns for TOFu and ~80 ns for the original DAQ. Given the record length of 64 samples (i.e. 64 ns) per record, out of which 16 samples are pre-trigger samples, the re-arm time between pulses of the TOFu DAQ can be calculated to ~12 ns. Another advantage of TOFu over the previous DAQ can be seen in the structure in the blue line (and lack of structure in the black line) extending down

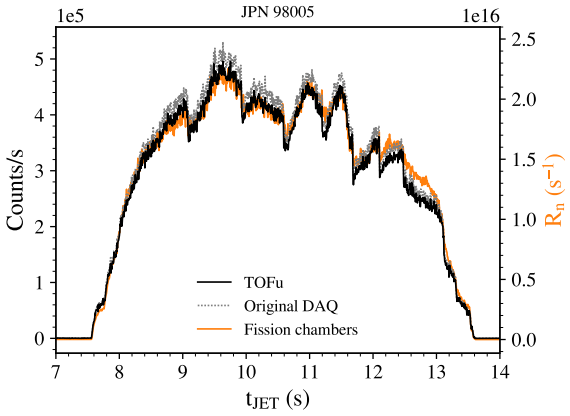

Fig. 12. The left vertical axis shows the count rates as a function of JET time for sub-detector S1-01 for TOFu (black line), and the previous TOFOR DAQ system (gray dotted line). The right vertical axis shows the total neutron emission rate as measured by the JET fission chambers (orange line).

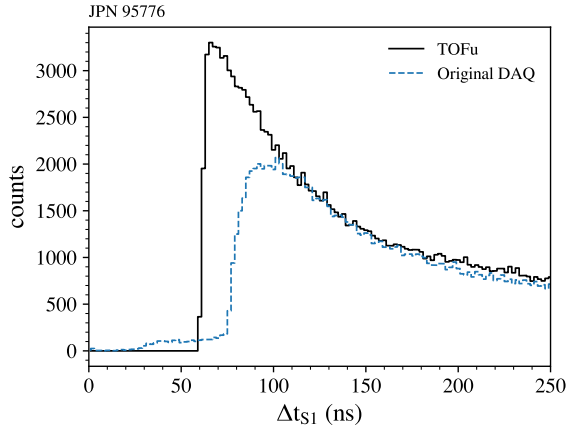

Fig. 13. Histogram of the shortest time differences between detected pulse waveforms for TOFu (black line) and the original DAQ (blue dashed line) for all S1 sub-detectors.

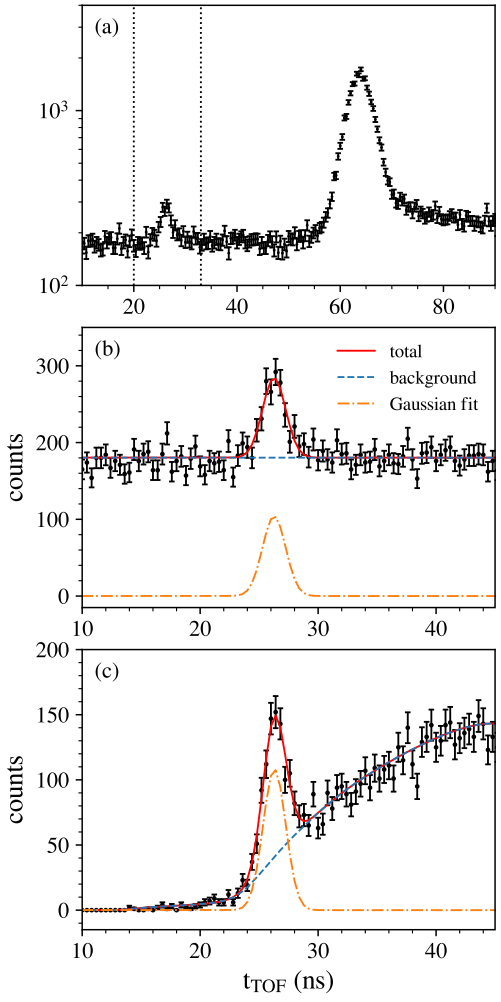

Fig. 14. (a) Full time-of-flight spectrum for JPN 100850 with the DT neutron peak indicated by the dotted black lines. Estimates of the background component (blue dashed lines) and a Gaussian fit to the DT neutron signal (orange dash-dotted lines) are applied to the DT peak with (b) no background discrimination and, and, (c) after utilizing kinematic cuts to discriminate against the background.

to $\Delta t_{S1} = 0$. For the original DAQ, the sub-detector channels are not entirely independent of each other in the series of FIFOs, constant fraction discriminators, and pulse logic units. Consequently, the pulse time-of-arrival can be incorrectly determined, typically during high count rate scenarios, when two events occur in two dependent channels within a short time span. Such problems are not present with the TOFu DAQ system as the time determination is performed independently for all channels.

9.2. Signal-to-background ratio

With the new TOFu DAQ system, we can utilize kinematic cuts as a powerful tool to discriminate against the background, as is exemplified for JPN 100850 in Fig. 9. Background discrimination using kinematic cuts is especially effective in increasing the signal-to-background ratio for small signals in large amounts of background (which is the case for the DT neutron peak in JPN 100850), as can be seen in Fig. 14 where the full TOF spectrum of JPN 100850, with no kinematic cuts applied, is shown in panel (a), and the DT peak is indicated by the black dotted lines. Since no background discrimination is employed the background forms a flat constant level visible as the blue dashed line in panel (b). The signal contributing to the DT peak is estimated by a Gaussian fit, shown as the orange dash-dotted line. In panel (c), background discrimination with kinematic cuts is applied to the same data set, significantly reducing the background component with respect to the signal. The signal-to-background ratio is calculated by integrating the background and signal components within a $\pm 3\sigma$ range of the Gaussian distribution, yielding an S/B ratio of 0.18 in panel (b) and 0.86 in panel (c), i.e., a relative improvement of almost 400%. Enhancing the DT signal to such a degree should improve the capability of TOFOR to perform fuel ion ratio measurements over a broader range of T fractions. A similar analysis is performed for JPN 99552 in which the tritium content in the plasma is significantly higher, resulting in a small DD neutron signal in a high level of background, as is shown in panel (a) of Fig. 15 where the DD neutron peak is indicated by the dotted black lines. The signal components are fit to the data without and with background discrimination in panels (b) and (c) respectively, and integrated between 57 and 72 ns along with the background components, yielding an S/B ratio of 0.42 in panel (b) and 1.24 in panel (c), i.e., an improvement of almost 200%. The background, here, consists of random coincidences, neutrons scattering in the tokamak walls (mainly from back-scattering in the divertor), and the low-energy tail of 14 MeV neutrons which have undergone multiple elastic collisions. Due to the shape of the applied kinematic cuts, a considerable amount of the background in the low-energy (high-TOF) side of the spectrum is removed from the DD peak when applying the background discrimination, which should improve our capability to perform spectroscopic analysis on the DD neutron peak.

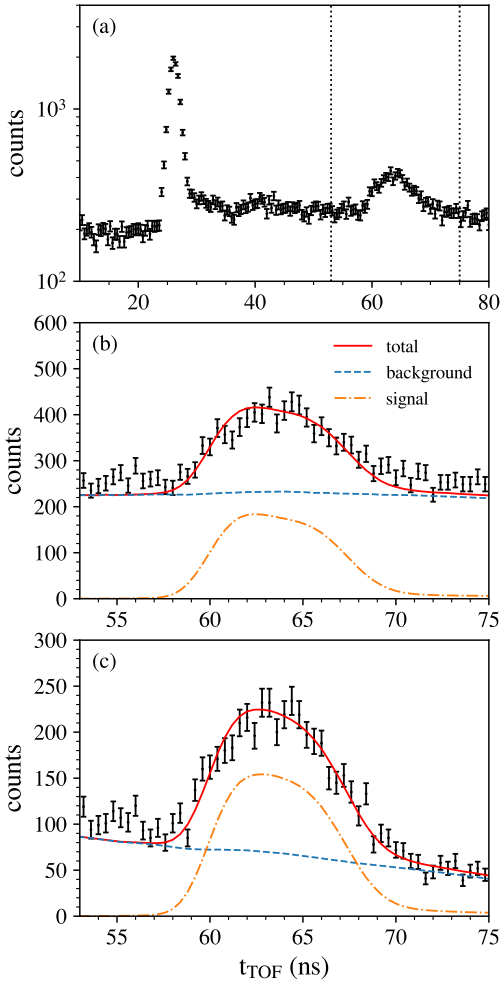

Fig. 15. (a) Full time-of-flight spectrum for JPN 99552 with the DD neutron peak indicated by the dotted black lines. Estimates of the background component (blue dashed lines) and a fit to the DD neutron signal (orange dash-dotted lines) are applied to the DD peak with (b) no background discrimination, and, (c) after utilizing kinematic cuts to discriminate against the background.

10. Conclusions

The upgraded TOFOR data acquisition system TOFu has been described in detail. The possibility of correlating energy and time information enables a more detailed post-analysis of the data than was previously available. Aspects of the post-analysis possible with the new system, as opposed to the previous DAQ system, include, e.g., a set of pulse selection criteria, an improved time pick-off method, and the use of kinematic cuts by performing a light yield calibration of the system. Two JET discharges are used to show an improvement in the S/B ratio of almost 200% and 400% for the 2.5 MeV and 14 MeV neutron signals through the use of kinematic cuts. Improvements of the S/B ratio to such a degree should improve the range over which we can perform fuel ion ratio measurements as well as our capability of performing spectroscopic analysis of the 2.5 MeV DD peak. Further, the TOFOR detector response function has been improved by including the individual time resolution and energy thresholds of each sub-detector. TOFu is a compact and flexible DAQ system that can be easily set up to fit the requirements for digitizing incoming pulse waveforms. The flexibility of the system was demonstrated during the deuterium–tritium experimental campaign (DTE2) at JET at the end of 2021 during which TOFu was moved and reinstalled in a few days at an entirely different spectrometer (the magnetic proton recoil spectrometer) and used to monitor the high power DT experiments. After DTE2, TOFu was moved back to TOFOR and is operating reliably on a daily basis.

Declaration of competing interest

The authors declare that they have no known competing financial interests or personal relationships that could have appeared to influence the work reported in this paper.

Data availability

Data will be made available on request.

Acknowledgments

This work has been carried out within the framework of the EUROfusion Consortium, funded by the European Union via the Euratom Research and Training Programme (Grant Agreement No 101052200 - EUROfusion). Views and opinions expressed are however those of the author(s) only and do not necessarily reflect those of the European Union or the European Commission. Neither the European Union nor the European Commission can be held responsible for them.

References

[1] M. Gatu Johnson, L. Giacomelli, A. Hjalmarsson, M. Weiszflog, E.A. Sundén, S. Conroy, G. Ericsson, C. Hellesen, J. Källne, E. Ronchi, et al., The TOFOR neutron spectrometer and its first use at JET, Rev. Sci. Instrum. 77 (10) (2006) 10E702.

[2] M.G. Johnson, L. Giacomelli, A. Hjalmarsson, J. Källne, M. Weiszflog, E.A. Sundén, S. Conroy, G. Ericsson, C. Hellesen, E. Ronchi, et al., The 2.5-MeV neutron time-of-flight spectrometer TOFOR for experiments at JET, Nucl. Instrum. Methods Phys. Res. A 591 (2) (2008) 417–430.

[3] M.G. Johnson, S. Conroy, M. Cecconello, E.A. Sundén, G. Ericsson, M. Gherendi, C. Hellesen, A. Hjalmarsson, A. Murari, S. Popovichev, et al., Modelling and TOFOR measurements of scattered neutrons at JET, Plasma Phys. Control. Fusion 52 (8) (2010) 085002.

[4] J. Eriksson, C. Hellesen, F. Binda, M. Cecconello, S. Conroy, G. Ericsson, L. Giacomelli, G. Gorini, A. Hjalmarsson, V. Kiptily, et al., Measuring fast ions in fusion plasmas with neutron diagnostics at JET, Plasma Phys. Control. Fusion 61 (1) (2018) 014027.

[5] C. Hellesen, M.G. Johnson, E.A. Sundén, S. Conroy, G. Ericsson, E. Ronchi, H. Sjöstrand, M. Weiszflog, G. Gorini, M. Tardocchi, et al., Neutron emission generated by fast deuterons accelerated with ion cyclotron heating at JET, Nucl. Fusion 50 (2) (2010) 022001.

[6] M.G. Johnson, C. Hellesen, E.A. Sundén, M. Cecconello, S. Conroy, G. Ericsson, G. Gorini, V. Kiptily, M. Nocente, S. Pinches, et al., Neutron emission from beryllium reactions in JET deuterium plasmas with 3He minority, Nucl. Fusion 50 (4) (2010) 045005.

[7] C. Hellesen, M. Albergante, E.A. Sundén, L. Ballabio, S. Conroy, G. Ericsson, M.G. Johnson, L. Giacomelli, G. Gorini, A. Hjalmarsson, et al., Neutron spectroscopy measurements and modeling of neutral beam heating fast ion dynamics, Plasma Phys. Control. Fusion 52 (8) (2010) 085013.

[8] B. Eriksson, S. Conroy, G. Ericsson, J. Eriksson, A. Hjalmarsson, Z. Ghani, I. Carvalho, I. Jepu, E. Delabie, M. Maslov, et al., Determining the fuel ion ratio for D(T) and T(D) plasmas at JET using neutron time-of-flight spectrometry, Plasma Phys. Control. Fusion 64 (5) (2022) 055008.

[9] B. Eriksson, Neutron time-of-flight spectrometry of fusion plasmas at JET: data acquisition developments and physics results (Ph.D. thesis), Uppsala University, 2022.

[10] M. Skiba, G. Ericsson, A. Hjalmarsson, C. Hellesen, S. Conroy, E. Andersson-Sundén, J. Eriksson, J. Contributors, A prototype fully digital data acquisition system upgrade for the TOFOR neutron spectrometer at JET, Nucl. Instrum. Methods Phys. Res. A 833 (2016) 94–104.

[11] FWPD - Real-time pulse detection firmware https://www.spdevices.com/products/firmware/fwpd (Accessed: 2022-07-07).

[12] B. Eriksson, TOFu analysis software, 2022, https://github.com/eriksson-benjamin/TOFu,

[13] B. Eriksson, S. Conroy, G. Ericsson, J. Eriksson, L. Giacomelli, A. Hjalmarsson, M. Weiszflog, J. Contributors, New method for time alignment and time calibration of the TOFOR time-of-flight neutron spectrometer at JET, Rev. Sci. Instrum. 92 (3) (2021) 033538.

[14] J. Valldor-Blücher, Upgrading the Control and Monitoring system for the TOFOR neutron time-of-flight spectrometer at JET, 2013.
[15] M. Tardocchi, G. Gorini, D. Palma, C. Sozzi, J. Källne, S. Conroy, G. Ericsson, L. Giacomelli, W. Glasser, H. Henriksson, et al., Control and monitoring system for fusion neutron spectroscopy on the Joint European Torus, Rev. Sci. Instrum. 75 (10) (2004) 3543–3546.
[16] C.E. Shannon, Communication in the presence of noise, Proc. IRE 37 (1) (1949) 10–21.
[17] C.J. Werner, et al., MCNP Users Manual-Code Version 6.2, Los Alamos National Laboratory, Los Alamos, 2017.
[18] C. Werner, J. Bull, C. Solomon, F. Brown, G. McKinney, M. Rising, D. Dixon, R. Martz, H. Hughes, L. Cox, et al., MCNP 6.2 release notes, 2018, Los Alamos National Laboratory, Report la-UR-18–20808.
[19] H. Klein, Neutron spectrometry in mixed fields: NE213/BC501A liquid scintillation spectrometers, Radiat. Prot. Dosim. 107 (1–3) (2003) 91–106.
[20] B. Eriksson, TOFu gamma calibration, 2022, https://github.com/eriksson-benjamin/gamma_calibration,
[21] M. Skiba, G. Ericsson, A. Hjalmarsson, C. Hellesen, S. Conroy, E. Andersson-Sundén, J. Eriksson, J. Contributors, Kinematic background discrimination methods using a fully digital data acquisition system for TOFOR, Nucl. Instrum. Methods Phys. Res. A 838 (2016) 82–88.
[22] B. Eriksson, TOFu time resolution, 2022, https://github.com/eriksson-benjamin/tofu_time_resolution,
[23] M. Gatu Johnson, Fusion plasma observations at JET with the TOFOR neutron spectrometer: instrumental challenges and physics results (Ph.D. thesis), Acta Universitatis Upsaliensis, 2010.
[24] P. Batistoni, S. Popovichev, Z. Ghani, A. Cufar, L. Giacomelli, P. Hawkins, K. Keogh, S. Jednorog, E. Laszynska, S. Loreti, et al., 14 MeV calibration of JET neutron detectors—phase 2: in-vessel calibration, Nucl. Fusion 58 (10) (2018) 106016.
[25] M. Skiba, M. Weiszflog, A. Hjalmarsson, G. Ericsson, C. Hellesen, S. Conroy, E. Andersson-Sundén, J. Eriksson, F. Binda, JET-EFDA Contributors, Fully digital data acquisition system for the neutron time-of-flight spectrometer TOFOR at JET, Rev. Sci. Instrum. 83 (10) (2012) 10D907.